

Article

Experimental Studies and Condition Monitoring of Auxiliary Processes in the Production of Al₂O₃ by Sol–Gel Technology

Vsevolod Sklabinskyi ¹, Oleksandr Liaposhchenko ¹, Ján Piteľ ^{2,*}, Ivan Pavlenko ¹, Maksym Skydanenko ¹, Ruslan Ostroha ¹, Mykola Yukhymenko ¹, Kostiantyn Simeiko ³, Maryna Demianenko ⁴, Michal Volf ⁴, Oleksandr Starynskyi ⁵, Oleksandr Yurchenko ¹ and Oleksandr Mandryka ¹

¹ Faculty of Technical Systems and Energy Efficient Technologies, Sumy State University, 2 Rymkogo-Korsakova St., 40007 Sumy, Ukraine

² Faculty of Manufacturing Technologies, Technical University of Košice, 1 Bayerova St., 080 01 Presov, Slovakia

³ The Gas Institute of National Academy of Sciences of Ukraine, 39 Dehtyarivska St., 03113 Kyiv, Ukraine

⁴ Faculty of Electrical Engineering, University of West Bohemia, 22 Univerzitni, 32600 Plzen, Czech Republic

⁵ Bobcat Doosan EMEA s.r.o., 1810 U Kodetky, 26312 Dobris, Czech Republic

* Correspondence: jan.pitel@tuke.sk; Tel.: +421-556026455

Abstract: Powders and granules of heavy metal oxides produced through condition monitoring are in high demand as intermediate products for obtaining fine-grained ceramics for a wide range of applications, i.e., nuclear fuel and fuel elements for nuclear power plants. Sol–gel technology to produce nuclear fuel (UO₂), as well as catalysts (ThO₂) for organic synthesis in the form of granules from pressed microspheres, is a promising method to obtain powders and granules of heavy metal oxides (fine-graded ceramics). Al₂O₃ was selected as the model analog at the stages of obtaining a solution of heavy metal and sol, the formation and gelation of droplets, and the preparation of gel spheres and their further washing and drying, as well as recovery and firing of particles. In the study, the main parameters were substantiated, e.g., the diameter and angle of inclination of the axis for the holes in the perforated shell, the multiplicity of sol circulation before the holes, the coefficients of liquid (sol) flow rate, the oscillation frequency of the disperser, and the concentration of surfactant and acid in sol. All of these parameters affect the characteristics of the granules that are obtained by sol–gel technology. Moreover, recommendations to increase productivity and the energy efficiency of production were also given. In particular, it was found that oscillation frequency in a range of 70–80 Hz leads to a granulometric composition of the obtained granules of 2.0–2.2 mm. A hole of 0.85 mm and a frequency of 100 Hz slightly change this range to 1.2–2.0 mm, while maintaining monodispersity.

Keywords: condition monitoring; sol–gel; granules formation; coil pulsation washer; microsphere; process innovation; energy efficiency



Citation: Sklabinskyi, V.; Liaposhchenko, O.; Piteľ, J.; Pavlenko, I.; Skydanenko, M.; Ostroha, R.; Yukhymenko, M.; Simeiko, K.; Demianenko, M.; Volf, M.; et al. Experimental Studies and Condition Monitoring of Auxiliary Processes in the Production of Al₂O₃ by Sol–Gel Technology. *Processes* **2022**, *10*, 2090. <https://doi.org/10.3390/pr10102090>

Academic Editor: Andrew S. Paluch

Received: 23 September 2022

Accepted: 12 October 2022

Published: 15 October 2022

Publisher's Note: MDPI stays neutral with regard to jurisdictional claims in published maps and institutional affiliations.



Copyright: © 2022 by the authors. Licensee MDPI, Basel, Switzerland. This article is an open access article distributed under the terms and conditions of the Creative Commons Attribution (CC BY) license (<https://creativecommons.org/licenses/by/4.0/>).

1. Introduction

The sol–gel process is a technology that can be applied in the nuclear industry to produce various types of radioactive fuel materials. This technology plays an essential role as part of fuel preparation for high-temperature helium-cooled reactors [1]. At the same time, powders and granules of heavy metal oxides manufactured by using the sol–gel technology are also commonly used as a pre-product for producing fine-grained ceramics for a wide range of applications: nuclear fuel and fuel elements for nuclear power plants, particulate filters, structural ceramics, catalysts and their carriers, biomedical products (prostheses), and so on [2]. In Reference [3], the sol–gel technology, with the use of a wide range of precursors, is applicable in the processing of textiles to achieve excellent water-repellent properties, especially when mixtures and hybrid precursors are used, as well as with the addition of various nanoparticles.

Powders and nanomaterials produced by using the sol–gel method are characterized by a monodisperse composition, single-phase crystal structure, strictly stoichiometric composition, and the absence of foreign phases. With the sol–gel process as the head-end process for fuel fabrication, the handling of radioactive, toxic powder is eliminated [3].

It is noted in Reference [4] that bioactive glasses and glass ceramics obtained from sol–gel represent a wide new area of bioactive materials with numerous applications in medicine and dentistry. The process of producing Al_2O_3 granules by the sol–gel technology includes several steps independent of the field of application, such as sol preparation, sol dispersion into drops, sol droplet settling in an aqueous solution, further curing, washing of gel spheres, drying, and annealing of granules (Figure 1). Many works describe this process [5,6]. The monodispersity of the granules and their physicochemical properties (strength, sphere diameter, porosity, specific surface area, and bulk density) depend on the raw material properties and individual characteristics of the sol–gel-process stages [7].



Figure 1. Sol–gel-process steps for producing Al_2O_3 granules.

The effect of the values of the gel-washing technological and operating parameters on the final properties of xerogel was determined in Reference [8]. The washing conditions were studied by changing the number of washes and the solvent (water or ethanol) to determine that the most significant efficiency (95%) was achieved with water and two washes. The physical, chemical, and structural properties of washed and unwashed xerogels are compared and discussed.

The possibility of using $\text{Th}(\text{NO}_3)_4$, with sulfate impurities, as raw material for the manufacturing of ThO_2 and $(\text{Th}, \text{U})\text{O}_2$ microspheres by the sol–gel process was considered in Reference [9]. In addition, the behavior and degree of sulfur removal during the process were determined.

Ganguly [10] investigated sol–gel microsphere pelletization (SGMP) to manufacture oxide, monocarbide, and mononitride fuel pellets with controlled density and microstructure. The SGMP line has advantages over the line for powder granules, namely the remote, automated, and economical production of ceramic nuclear fuel and high-radiation toxic fuel granules to eliminate oxides, carbides, and nitrides, in particular, Pu and ^{233}U . References [11,12] present the results of a series of multi-stage studies in which microspheres of uranium dioxide with a diameter of fewer than $100\ \mu\text{m}$ were obtained by using a stopped sol–gel complex, using granules in an oxygen-free environment. Thus, the optimal calcination temperature of $700\ ^\circ\text{C}$, with a low heating rate of $2\ ^\circ\text{C}/\text{min}$, and a maximum temperature of $900\ ^\circ\text{C}$ in an oxygen-free environment for the reduction process were determined, making it possible to avoid the formation of cracks on the surface of UO_2 microspheres in a cubic-type crystal structure.

It should be noted that the research work [13] paid attention to most of the stages of the sol–gel process, the formation of microspheres in the gelation column, their washing, drying, and their effect on the quality of the target product, namely monodispersity, porosity, the presence of impurities, and the size of the microspheres. In Reference [14], the influence of heating processes on the properties and microstructure of porous CeO_2 spheres as a surrogate for nuclear fuel produced by the microfluidic sol–gel process was considered. Heating regimes and peak temperatures for CeO_2 calcination were studied to optimize porous microspheres' mechanical properties and microstructure.

In Reference [15], the process of manufacturing CeO₂ microspheres by internal gelation was studied by using a T-junction droplet generator. This study used T-junction-droplet generators with 0.5, 0.8, 1.0, and 3.0 mm inside channel diameters to disperse the droplets. The influence of the flow rate of the continuous and dispersed phases on the size and size distribution of Cerium (Ce) microspheres was determined, and several correlations were developed that are useful for predicting droplet diameters in T-junction geometry. Other results in studying the impact of properties for oxides and catalysts were presented in References [16–19].

In References [20,21], new methods were presented to produce Al₂O₃ thin films based on the sol–gel method. Al₂O₃ films produced by the sol–gel process exhibit excellent optical, electrical, and adhesive properties and are crack-free.

In another study [22], a droplet-based microfluidic reaction scheme was developed in which chemical reagents were distributed with precise volume control into droplet pairs. The reaction is activated by the coalescence of the droplet pairs and rapid mixing within the coalesced droplets. Using this approach and optimizing the reaction parameters, mesoporous granules were generated. Silica microspheres from a an article sol–gel process were optimized for fast gelation.

It should be noted that, in most of the considered works, attention was not paid to the improvement of the equipment in the technological lines used to produce microspheres according to the sol–gel method, especially auxiliary equipment (devices for spraying sol in the gelation column, devices for washing gel spheres, dryers, etc.) Traditionally, to improve the quality of the target product, it is necessary to consider all possible modes of operation of individual pieces of equipment that go beyond the normal operation of the installation, as well as the acceleration of limiting technological processes.

During the operation of an industrial plant to produce Al₂O₃ microspheres (a liquid dispersant), the theoretical flow rate of the liquid may differ from the actual one. This fact is due to various factors, particularly deviation holes' axes and an uneven supply of liquid as a result of internal circulation.

In Reference [23], the process of external gel formation was developed for microspheres of ThO₂ and UO₂. For this purpose, a pre-neutralized solution of urea and ammonium nitrate or directly prepared Th sol was used. The droplets of these solutions turned into a gel in gaseous ammonia. The gel spheres were washed with an ammonia solution at 60 °C, dried on a belt dryer at 150–500 °C, and sintered at 1200 °C. This process is still applied to produce fuel from coated particles. However, the limitation of this process is the size of the final sintered product, which cannot exceed 0.5 mm.

One of the well-studied methods for preparing gel microspheres of UO₂, ThO₂, (U, Pu)O₂, and (Th, U)O₂ is described in Reference [24]. Solutions of nitrates of uranium, thorium, plutonium, and their mixtures are used in the process. Chilled mixtures of metal nitrates at approximately 0 °C are mixed with urea solution CO(NH₂)₂ and (CH₂)₆N₄. The droplets of this mixture make contact with hot silicone oil at 90 °C to obtain gel microspheres. These gel microspheres are washed first with CCl₄ to remove silicone oil, and then they are washed with NH₄OH solution to remove gelling agents. The washed particles are dried at 150 °C in air and then fired at 500 °C to remove the remains of organic matter and ammonium nitrate. Then the calcined microspheres are restored at 600 °C. The resulting UO₂ microspheres are sintered at 1200 °C for 3 h.

An innovative fast sol–gel method to produce hydroxyapatite nanopowders was developed in Reference [25]. It avoids drying processes and is 200 times faster than conventional aqueous sol–gel and 50 times faster than ethanol-based sol–gel synthesis. Moreover, two different sets of experimental conditions were investigated in terms of synthesis (45–90 °C), drying (60–80 °C), and calcination (400–700 °C) temperatures.

Overall, the study of leakage through round holes in the presence of additional factors, such as axis misalignment and flow swirling, can introduce adjustments into mathematical models and analytical dependencies and, on this basis, increase the reliability and efficiency of the developed method.

frequency, and rotational speed of the vibrating granulator on properties of the granules such as bulk density, strength, and monodispersity will be determined.

To determine the parameters of fluid outflow through the round holes in the thin wall, secondary breakup of dropping liquid, and the effect of superimposed vibrations on droplet oscillation modes in the prilling process, the recommendations presented in previous works [26–29] were used. There are practically no recommendations for determining the flow parameters in the presence of other conditions, such as the inclination of the orifice axis or the presence of flow circulation in front of the orifice. Special experimental setups for condition monitoring were designed and manufactured to study the questions posed (Figure 3a,b). The setup shown in Figure 3a allows for the study of jet leakage with and without tilting the hole. Tilting to a specific angle is achieved by tightening or unscrewing the screw in the tripod leg. The replacement of the reservoir changes the diameter of the openings.

With a constant circulation in the reservoir ($G = \text{const}$), liquid layers at different radii move with different peripheral speeds, which can be represented as a hyperbolic law along the radius:

$$V_u = G/2\pi r. \quad (1)$$

The condition for the existence of a vortex in a reservoir can be represented as follows:

$$(V_{uB})^2/2g = Z, \quad (2)$$

where Z is the distance from the free surface to the vortex section (m), V_{uB} is the circumferential velocity on the vortex surface in the vortex section (m/s).

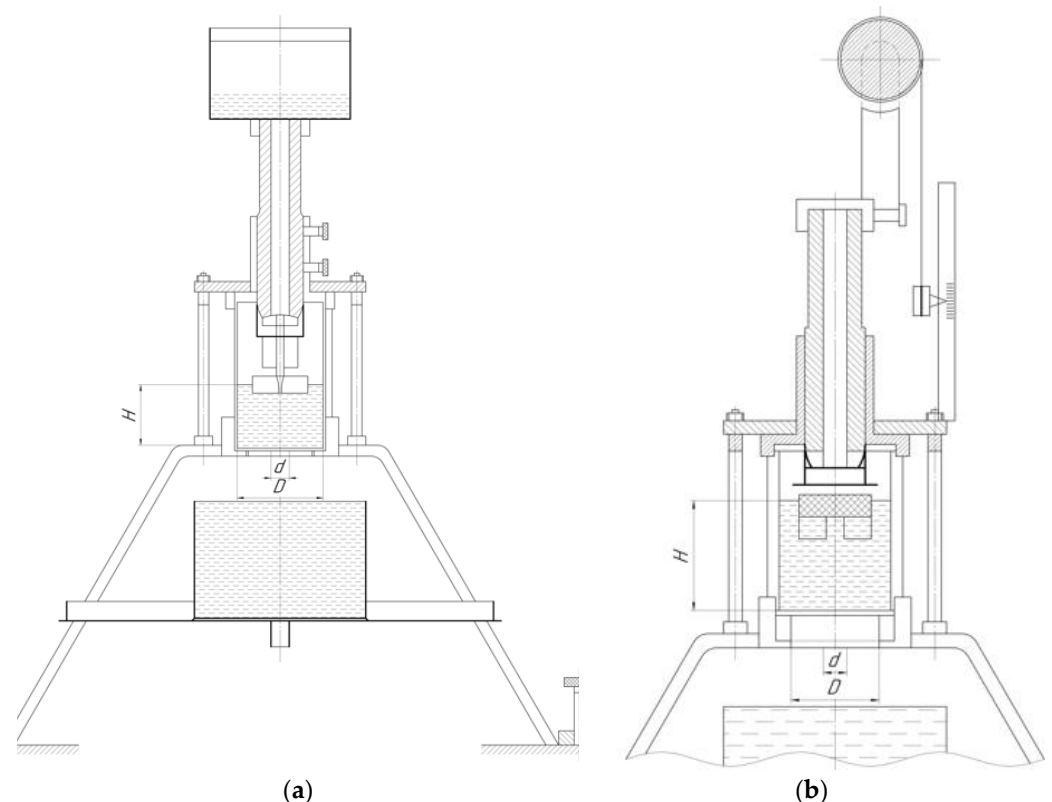


Figure 3. (a) Installation for studying the leakage of the jet, taking into account the inclination of the hole. (b) Installation for studying the jet leakage, taking into account the circulation in front of the hole.

The experimental setup to study the effect of circulation on runoff is shown in Figure 3b. This installation was assembled based on the installation shown in Figure 3a, with the

change that had a special reservoir with 20 nozzles evenly distributed along the height. The nozzles exited the reservoir tangentially, which made it possible to circulate in the reservoir. The pressure in the manifold (and, accordingly, the pressure in the nozzles) was controlled by using a piezometer. This made it possible to set the required pressure precisely. The change in pressure in the collector was carried out by throttling the water leaving the drain from the collector.

The following formula determines the flow rate when flowing through the hole:

$$Q = \mu F_o \sqrt{2gH}, \quad (3)$$

where μ is the coefficient of fluid flow through the hole, F_o is the hole's area (m^2), and H is the excess pressure above the hole (Pa).

The following expression determines the flow rate:

$$\mu = \varphi \delta, \quad (4)$$

where φ is the speed coefficient, and δ is the compression ratio at the hole outlet.

The value of the flow coefficient depends on many factors since it is influenced by all the factors associated with the jet compression coefficient and the velocity coefficient, φ .

Experimental studies of liquid flow through a hole in thin walls were carried out. Al_2O_3 sol was used as a working fluid. It should be noted that, in order to avoid clogging the holes during the experiment, the diameter of the hole in the reservoir was increased compared to the holes in the basket of the industrial dispersant (priller), i.e., 5.5, 8.0, 10.0, and 12.0 mm. In this case, the diameter of the reservoir is 60 mm.

The flow coefficients for other liquids and the effect of the liquid temperature have hardly been studied. After analyzing the recommendations of various authors on this issue, we present the most common recommendations for determining the coefficient, μ . The practical recommendations propose taking the following values of μ :

For $\text{Re} < 25$:

$$\mu = \varphi = \text{Re}/48. \quad (5)$$

At $25 < \text{Re} < 200\text{--}400$:

$$\mu = \text{Re}/(1.5 + 1.4*\text{Re}). \quad (6)$$

(The highest value of μ_{max} is 0.69; in some studies, the value $\mu_{\text{max}} = 0.72$ can be found, too.)

At $200\text{--}400 < \text{Re} < 10,000$:

$$\mu = 0.592 + 0.27/\sqrt{\text{Re}}. \quad (7)$$

At $10,000 < \text{Re} < 300,000$:

$$\mu = 0.592 + 0.27/\sqrt{\text{Re}}. \quad (8)$$

For $\text{Re} > 300,000$, the discharge coefficient remains almost unchanged and amounts to 0.595 or approximately 0.6. The Reynolds number, in this case, is calculated from the dependence, as follows:

$$\text{Re} = \sqrt{(2gH*d)/\nu}, \quad (9)$$

where d is the diameter of the hole [2], and ν is the kinematic viscosity of the liquid (m^2/s).

From Expressions (4)–(7), the flow coefficient should increase with an increase in the viscosity of the liquid. In the case of incomplete jet compression, the value of the flow coefficient, μ_H , will be greater than the flow coefficient, μ , for the case of full compression:

$$\mu_H = \mu(1 + c*n/x), \quad (10)$$

where c is a dimensionless coefficient that considers the shape of the holes (for round holes, it is 0.13; for rectangular holes, it is 0.15), n is the perimeter of that part of the contour of the holes on which there is no jet compression (m), and x is the hole perimeter (m).

Imperfect compression can be considered depending on the hole's area ratio, ω , and the total area for Ω in which the hole is located:

$$\mu_H = \mu[1 + 0.641 * (\omega / \Omega)^2]. \quad (11)$$

Therefore, using the available recommendations for condition monitoring, we calculated the flow rates for all termination cases and compared them with the experimental data. As regards the outflow of a jet with an inclination of the hole with pre-circulation, a detailed study of these issues, both experimentally and theoretically, is necessary.

One way to increase the efficiency of the gel-sphere-washing process is to use a pulsed one. For example, a serpentine washer (Figure 4a) works as follows: the gel spheres enter the coil through the inlet unit. Ammonia solution enters through the gel-sphere removal unit. The movement of the gel spheres and the ammonia solution is countercurrent. Hydraulic impulses generated by the pulsator carry out the gel spheres' movement in the coil.

The nature of the hydraulic impulses (Figure 4b) is such that, during the direct movement (i.e., upward) of the ammonia solution in the coil, its speed is less than the removal velocity of the gel spheres, and the gel spheres remain in place. During the reverse movement of the ammonia solution, its velocity is greater than the removal velocity, and the gel spheres move a certain distance. Since the hydraulic impulses are applied continuously, the movement of the gel spheres in the serpentine washer is continuous.

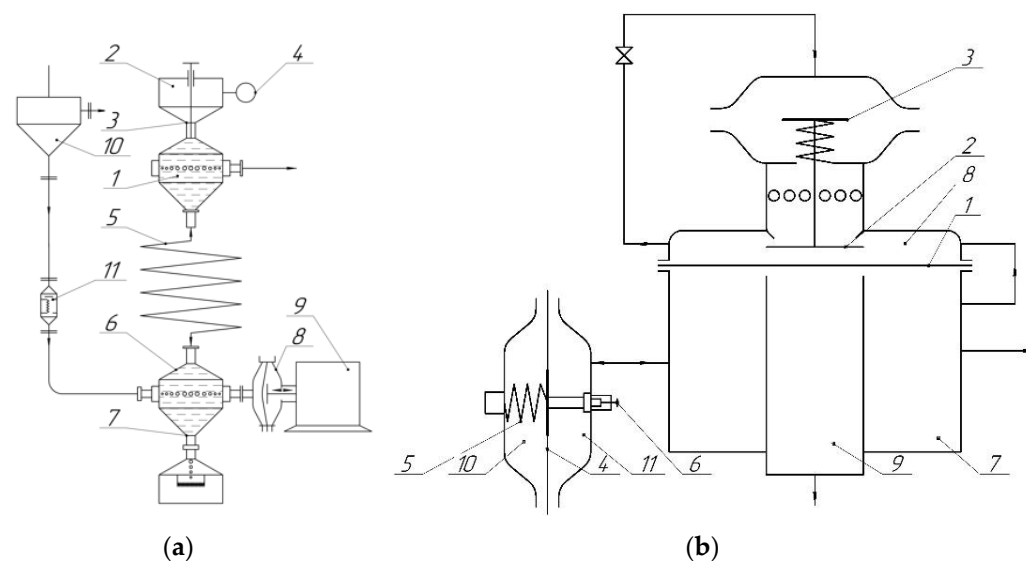


Figure 4. (a) Pulsating serpentine gel-sphere washer: 1—gel spheres injection node; 2—container with washing liquid; 3—pipe for supplying the washing liquid; 4—pump; 5—coil pipe; 6— gel sphere output node; 7—collector of the washed gel spheres; 8—pulsator; 9—drive; 10—pressure tank; 11—flow meter. (b) Pneumatic pulse generator: 1—flexible diaphragm; 2—valve; 3, 4—flexible diaphragms; 5—spring; 6—regulating screw; 7, 8— cavities; 9—exhaust pipe; 9—drive; 10, 11—cavities of the pulsator.

The main stage of the sol–gel process is spraying the sol into the ammonia–water solution. This step is carried out at gauge pressure in the spraying device (priller) and gauge pressure in the column. The experimental unit for studying the leakage of the jet considers the inclination of the hole and circulation in the tank. The experimental unit also considers pulsating serpentine for the gel-sphere washer, and the magnetostrictive

dispersion operates at atmospheric or gauge pressure. Vacuum pressure is absent in the equipment.

When studying the hydrodynamics of the process of washing gel spheres in a coil washer, it is necessary to conduct experiments to study the dependence of the speed of movement of the gel spheres in the coil on the following parameters: the frequency of movement of the diaphragm, $\omega_{cf} = \varphi(f)$; diaphragm movement amplitude, $\omega_{cf} = \varphi(A)$; average coil diameter, $\omega_{cf} = \varphi(D_p)$; and degree of filling of the coil, $\omega_{cf} = \varphi(K_c)$.

The studies are carried out by using the “cut-off” method, which is as follows: Washable gel spheres are fed into the coil at a constant flow rate. After the unit enters the mode and the coil is filled with sand, the coil is disconnected from the system, after which the gel spheres are unloaded from the coil, dried, and weighed.

By knowing the consumption of gel spheres and their number in the coil, it is possible to determine the coil’s filling time:

$$\tau_3 = G_4/Q_4, \quad (12)$$

where τ_3 is the coil’s filling time (s), Q_4 is the mass flow rate of the washed gel spheres (kg/s), and G_4 is the weight of particles in the coil (kg).

The average speed, ω_{av} , of movement of particles in the coil is as follows:

$$\omega_{av} = L/\tau_3, \quad (13)$$

where L is the length of the coil pipe (m).

The distance moved by the gel spheres in one stroke of the pulsator is determined by the following formula:

$$l = k(D^2)/(d_i^2) \quad (14)$$

where l is the displacement of the gel spheres in one stroke of the pulsator (m), D is the effective diameter of the pulsator diaphragm (m), d_i is the inner diameter of the coil pipe (m), and k is the impact of the boundary layer of the liquid.

The average speed, ω_{mv} , of movement of the gel spheres in the coil is determined by the following equation:

$$\omega_{mv} = fl, \quad (15)$$

where f is the frequency of the supplied hydraulic pulses.

Based on Equations (13) and (14), the gel spheres’ average velocity depends on the hydraulic pulses’ frequency and geometric characteristics of the pulsator and coil. Therefore, by changing these characteristics, it is possible to control the washing time of the gel spheres. This unit uses a diaphragm pulsator with a pneumatic drive (Figure 5), which excludes the possibility of leakage of the washing medium and provides a simple adjustment of the speed of movement of the gel spheres.

A promising method for sputtering sol particles is the magnetostrictive method. When working on small holes (0.1 mm or less), there is a high probability of their clogging by impurities, as well as due to gelation of the solution in the hole, which is possible at the achieved flow rates of the solution from the holes (up to 2.5–3.0 m/s). Therefore, the introduction of magnetostrictive vibrators of increased frequency up to ultrasonic frequencies in order to increase the gelling solution flow rate by 2 to 3 times is an urgent scientific problem. It should be assumed that, in this case, it will be possible to significantly reduce the probability of clogging the holes with impurities or gel particles by increasing the pressure and velocity of the solution in front of the holes and continuous ultrasonic or sonic cleaning of the holes and destroying the gel particles (in the case that they are prematurely created in front of the drain holes). In addition, using magnetostrictive vibrators makes it possible to make the dispersing device more compact and to increase the performance of dies several times.

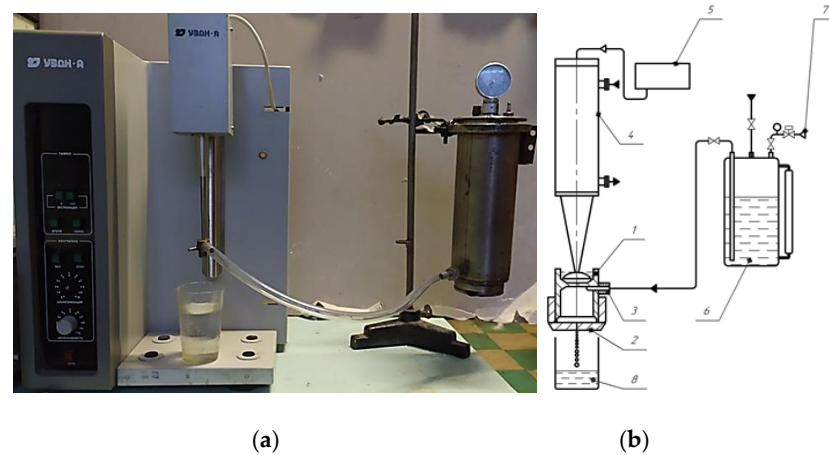


Figure 5. External view (a) and design scheme (b) of the installations for the study of the magnetostrictive method of the liquid dispersion: 1—dispersing head; 2—spinneret; 3—liquid supply fitting; 4—radiating part of the magnetostrictive vibrator; 5—generator; 6—container with raw materials; 7—pneumatic valve; and 8—collection container.

The basket's diameter selection for the holes depends on the diameter of the obtained granule. The smaller the diameter of the hole in the disperser basket, the smaller the granule diameter.

The frequency of forced oscillations imposed on sol jets also depends on the diameter of the obtained granules. Therefore, the frequency of forced oscillations should be chosen depending on the granulometric composition of the main fraction.

Furthermore, since the diameter of the jets is in the range of 0.85–1.40 mm, the main forces influencing the dispersion mode are surface tension forces. Therefore, it is expected that a larger monodisperse composition of granules can be obtained with a decrease in surface tension (due to the addition of surfactant). Simultaneously, a decrease in surface tension leads to the deformation of the sol droplet when interacting with the gel. Therefore, surfactant concentrations should be chosen thoroughly.

To determine the granulometric composition of Al_2O_3 , the experimental batch was weighed. A particle size analysis was carried out on sieves, using the vibrational sieve analyzer "ACB-300" (Figure 6).

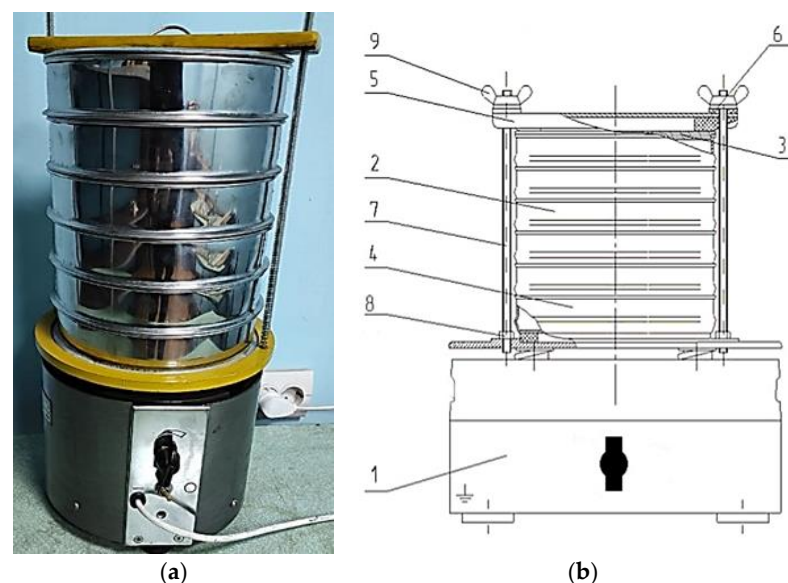


Figure 6. External view (a) and design scheme (b) of the particle-size analyzer: 1—vibration drive; 2—sieve; 3—cover; 4—pallet; 5—traverse; 6—clamp; 7—pin; 8—counter nut; and 9—nut.

A set of sieves with a tray and a cover is installed on the plate of the vibratory drive and fixed by the fastening device. The sieve is a round welded shell made of stainless steel, with a sieving element installed.

After turning on the vibration drive, its plate and a set of sieves perform reciprocating screw oscillations with the amplitude of the oscillation of the vibrating stand from 1.5 to 3.0 mm and the oscillation frequency of 2.6–50 Hz. The material moves along the sieving surface of the sieves from the center to the periphery in a spiral. Particles of material that are smaller than the size of the holes in the sieve's surface fall through it and fall onto the sieve located below, where the cycle is repeated.

The arrangement from sieves with large holes to sieves with small holes is typical. Sieves with the following hole diameters were used: 1.0, 1.2, 1.6, 1.8, 2.0, 2.2, 2.4, 2.5, 3.0, and 3.5 mm. As a result, the dispersed material is distributed between the sieves and the pallet in quantities that depend on its fractional composition. After sieving, the residue is taken from each sieve and weighed. The result of weighing is recorded to the first decimal place.

The mass fraction X (%) is determined as follows:

$$X = 100 \cdot m_1 / m, \quad (16)$$

where m is the probe mass (g), and m_1 is the mass of a fraction (g).

3. Results of Experimental Studies and Condition Monitoring

The production of Al_2O_3 catalyst granules was carried out on the experimental research equipment for condition monitoring shown in Figure 2. In the first series of studies, eight experiments were carried out (Table 1) at a sol flow rate of $2.37 \times 10^6 \text{ m}^3/\text{s}$, with a sol density of 1208 kg/m^3 . In the first two experiments, the diameter of the holes of the priller was 1.4 mm, and the oscillation frequency was 100 Hz, while the amount of surfactant added to the sol was 2–5 mL. The diameter of the obtained Al_2O_3 granules was 2.00 to 2.55 mm, the bulk density after drying the granules was 0.37 to 0.4 kg/m^3 , and after calcination, it was 0.34 to 0.39 kg/m^3 . Their strength was determined to be 1.2 to 1.9 kg/grain .

Table 1. Results of the first series of experiments on the production of Al_2O_3 granules.

| Exp. No. | Hole Diameter (mm) | Needle Length (mm) | Frequency (Hz) | Bulk Density (kg/m^3) | | Granules' Basic Fractions (mm) |
|----------|--------------------|--------------------|----------------|----------------------------------|-------------------|--------------------------------|
| | | | | after Drying | after Calcination | |
| 1 | 1.4 | 27 | 100 | 0.37/0.39 | 0.34/0.36 | 2.5 |
| 2 | 1.4 | 27 | 100 | 0.37/0.40 | 0.37/0.39 | 2.0–2.5 |
| 3 | 1.2 | 28 | 68 | 0.37/0.41 | | 2.0–2.2 |
| 4 | 1.2 | 28 | 40 | 0.38/0.40 | | 2.0–2.4 |
| 5 | 1.2 | 28 | 70–80 | 0.35/0.39 | | 2.0–2.2 |
| 6 | 1.0 | 31 | 42 | | | 1.2–3.0 |
| 7 | 1.0 | 32 | 100 | 0.35/0.37 | | 1.2–2.2 |
| 8 | 0.85 | 33 | 100 | 0.37/0.40 | 0.34/0.36 | 1.2–2.0 (1.6) |

In the third experiment, the diameter of the holes was 1.2 mm, the amount of surfactant was 2 mL, and the oscillation frequency of the actuator was 68 Hz. It should be noted that, in this experiment, the length of the continuous jet was 65 mm. As a result, granules with a diameter of 2.0 to 2.2 mm were obtained, and their bulk density after drying was 0.37 to 0.41 kg/m^3 . In the fourth experiment, the holes' diameter and the surfactant amount did not change, and the oscillation frequency was reduced to 40 Hz. The length of the continuous jet was 35 to 40 mm. The catalyst granule diameter was 2.0 to 2.4 mm, and their bulk density after drying was 0.38 to 0.40 kg/m^3 . During the fifth experiment, the oscillation frequency was increased to between 70 and 80 Hz, and the amount of surfactant was increased to 12 mL, while 40 mL of water was added to the sol. The length of the

continuous jet under these operating conditions was 20 to 30 mm. The catalyst granule diameter was 2.0 to 2.2 mm, and the bulk density after drying was 0.35 to 0.39 kg/m³.

In the sixth experiment, the hole diameter was 1.0 mm, and the oscillation frequency was 48 Hz. With these parameters, a polydisperse composition of granules of 1.2 to 3 mm was obtained. Therefore, increasing the oscillation frequency in the seventh experiment up to 100 Hz was decided. At this frequency, and after adding 12 mL of surfactant to the sol with the length of the continuous jet 20 mm, it was possible to obtain granules with a diameter of 1.2 to 2.2 mm, with a bulk density after drying of 0.35 to 0.37 kg/m³.

In the eighth experiment, the diameter of the disperser holes was 0.85 mm, the oscillation frequency was 100 Hz, the amount of surfactant was 8 mL, and the amount of water was 90 mL. During dispersion, the length of the continuous jet was 45 mm. The diameter of the granules obtained with the given operating parameters of the installation was 1.2 to 2.0 mm, while most of the granules of Al₂O₃ were monodisperse aluminum with a diameter of 1.6 mm. The bulk density after drying the granules was 0.37 to 0.40 kg/m³, and after calcination, it was 0.34 to 0.36 kg/m³. The strength of the pellets was also determined to be 0.846 kg/grain.

During the second series, the acid concentration and powder–acid ratio (Al(OH)₃:HNO₃) were determined for the granules' strength and bulk density after calcination. Thus, eight experiments were carried out in which the diameter of the disperser holes was 1.0 mm, the rotation frequency was 30 rpm, and the oscillation frequency was 60 Hz. An additional experiment was also carried out in a more intense hydrodynamic mode in which the diameter of the holes was 0.8 mm, the rotation frequency was 60 rpm, and the oscillation frequency was 90 Hz. The experimental results are summarized in Table 2.

Table 2. Results of the second series of experiments on the production of Al₂O₃ granules.

| Exp. No. | Conc. Ki-Slots, n | Attitude Powder/Acid | Granules' Basic Fractions (mm) | Bulk Density (kg/m ³) | Strength (kg/gran.) |
|----------|-------------------|----------------------|--------------------------------|-----------------------------------|---------------------|
| 1 | 0.476 | 1:2 | 2.5–3.0 | 318 | 1.5 |
| 2 | 0.445 | 1:2 | 2.0–2.2 | 371 | 1.2 |
| 3 | 0.428 | 1.05:2 | 2.5–3.0 | 356 | 1.5 |
| 4 | 0.483 | 1.05:2 | 2.0–3.0 | 375 | 1.8 |
| 5 | 0.467 | 1.05:2 | 2.0–2.5 | 370/358 | 1.2 |
| 6 | 0.43 | 1:2 | 2.0–2.5 | 360/353 | 1.2 |
| 7 | 0.43 | 2.0:3.5 | 2.0–2.5 | 372/354 | 1.0 |
| 8 | 0.415 | 2.0:3.66 | 2.0–2.5 | 373 | 1.1 |
| 9 | 0.43 | 1:2 | 1.6–1.8 | 371 | 1.2 |

As mentioned above, the purpose of the experiment was to determine the flow coefficient, μ , for different values of the Reynolds numbers, Re (or for the heights of the liquid column in the reservoir), under different outflow conditions. The flow rate can be written as follows:

$$\mu = Q_R / Q_T, \quad (17)$$

where Q_R is the actual flow through the hole, and Q_T is the theoretical flow through the hole.

The actual flow rate is determined by the following volumetric method:

$$Q_R = W/t \times 10^{-3}, \quad (18)$$

where W is the volume of the measuring tank (L), and t is the filling time of the measuring tank (s).

The following formula determines the theoretical flow:

$$Q_T = \mu_T * F_o \sqrt{2gh} \quad (19)$$

where μ_T is the theoretical flow coefficient, which, in the absence of losses, is equal to 1; F_o is hole's area (m^2); and h is the liquid column's height (m).

As for studies with circulation, the generally accepted criteria are not suitable. The following formula determines the Reynolds number:

$$Re = (V_{ub} \cdot d) / \nu \quad (20)$$

It is not known how to determine the theoretical flow, namely how to substitute the area F_o in Formula (19) to determine the theoretical flow. Here, it can be performed differently, for example, when F_o conditionally takes the area of the hole. Then, at high circulations, when the flow rate through the orifice approaches zero, obviously, the flow coefficient approaches infinity since the theoretical flow rate will always remain a finite value (at $h > 0$). Consequently, such a problematic F_o will not characterize the flow. It is advisable to take the annular area formed by the holes of the walls and the surface of the vortex as the area F_o . Then, with an increase in circulation, according to Condition (2) for the existence of a vortex, its diameter should increase. Therefore, the annular area will decrease. This will reduce both the actual flow rate and the theoretical flow rate; hence, the flow factor will always remain the final value.

While processing the experimental results, Dependence (20) was used to determine the Reynolds number. The circumferential velocity of the vortex was determined from Condition (2), and the flow rate was determined from Equation (17). Correction factors were calculated to obtain results convenient for practical use, which must be entered to refine the flow coefficients, μ . These coefficients are the ratio of the flow coefficient obtained empirically to the coefficient and flow determined by analytical dependencies:

$$K_\alpha = \mu_o / \mu_m \quad (21)$$

The results of experimental studies are shown in Figures 7–13. Graphs are constructed for different angles α (the angle of inclination of the plane of the hole to the horizontal) and different hole diameters for the cup diameter, d/D . It should be noted that no leakage occurs at the relatively low Reynolds numbers. This fact gives considerable uncertainty to the flow coefficient, μ .

The flow coefficient practically does not change at $Re > 10^5$. When $Re < 10^5$, the flow coefficient, μ , has a complicated dependence, and its determination can be made according to various recommendations. In this case, the termination occurs at values of $Re < 10^5$. Therefore, it becomes clear how important it is to choose a dependence that would give good agreement with the experiment. By analyzing the graphs shown in Figures 7–10, we can see that the values obtained from the experimental results differ from the calculated (theoretical) ones. Moreover, the flow coefficient, μ , also depends on the angle of inclination of the hole plane to the horizontal plane. Therefore, calculating the coefficient according to the recommendations for $Re < 10^5$ can lead to inaccuracies. Therefore, concerning the coefficient, μ , it is advisable to use the correction factors shown in Figures 11–13. It should be noted that the indicated coefficients are valid only when the flow coefficient, μ , is calculated according to the recommendations. Therefore, in order to more accurately determine the value of μ , it is necessary to calculate the theoretical coefficient, μ_T , according to the recommendations and then multiply it by the corresponding value of K_α taken from the graphs (Figures 11–13):

$$\mu = K_\alpha \cdot \mu_m \quad (22)$$

As the experiments show, even a slight circulation in the reservoir significantly affects the leakage of liquid from the hole. For studies with circulation, the flow was determined for several values of circulations at different values of h and d/D . The results are summarized in the table in Appendix A. For comparison, the same table shows the cost values for the same values of h and the ratio d/D , but without circulation.

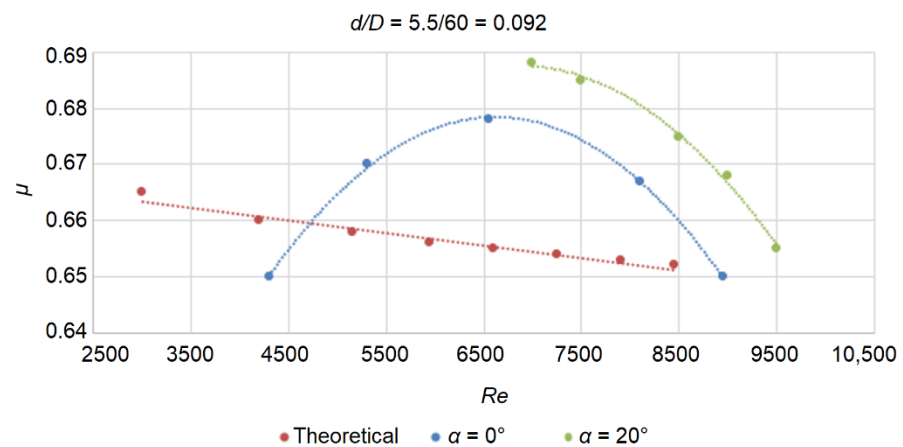


Figure 7. Dependence of liquid (sol) flow rates, μ , through the hole on the criterion Re ($2000 < Re < 11,000$), with the ratio $d/D = 5.5/60 = 0.092$.

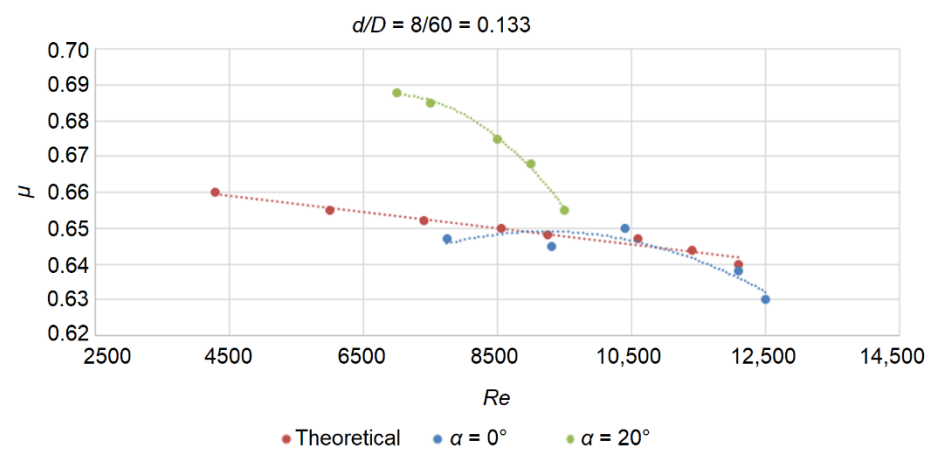


Figure 8. Dependence of the coefficients of liquid (sol) flow rate, μ , through the hole on the criterion Re ($4000 < Re < 13,000$), with the ratio $d/D = 8/60 = 0.133$.

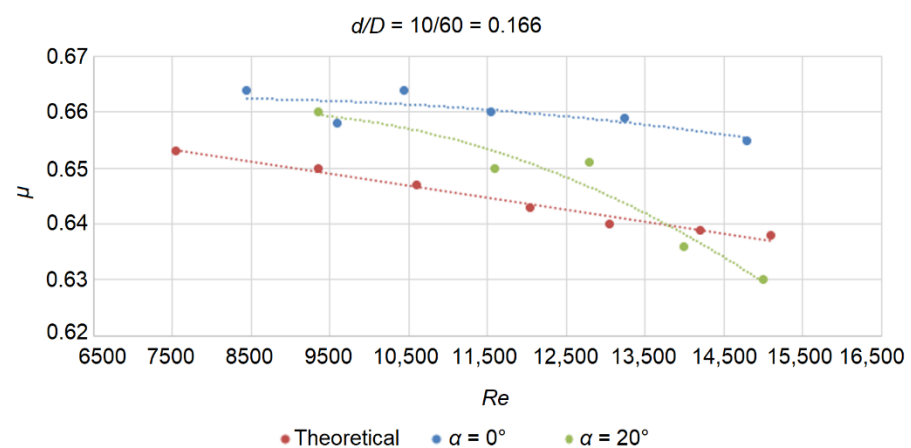


Figure 9. Dependence of the coefficients of liquid (sol) flow rate, μ , through the hole on the criterion Re ($5000 < Re < 17,000$), with the ratio $d/D = 10/60 = 0.166$.

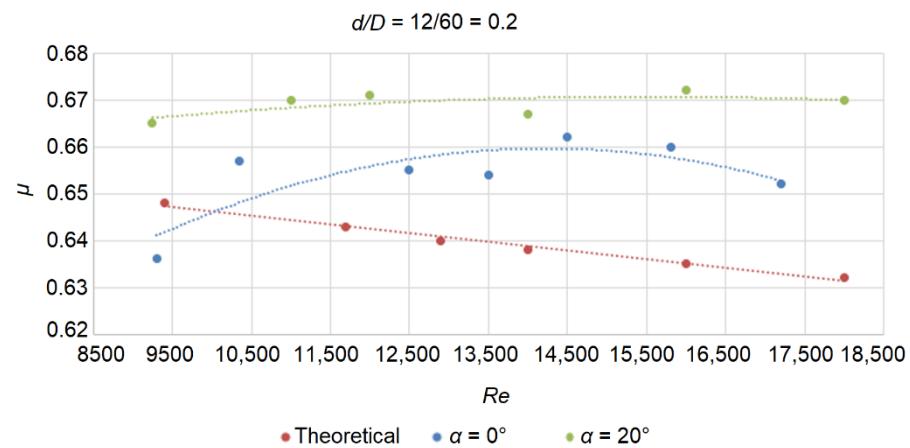


Figure 10. Dependence of the coefficients of liquid (sol) flow rate, μ , through the hole on the criterion Re ($9000 < Re < 19,000$), with the ratio $d/D = 12/60 = 0.2$.

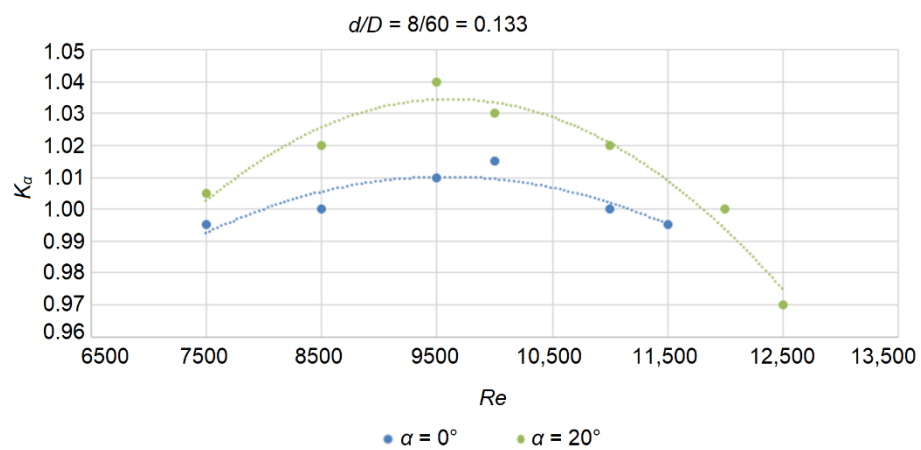


Figure 11. Dependence of the correction factors, K_{α} , on the criterion Re ($7000 < Re < 13,000$), with the ratio $d/D = 8/60 = 0.133$.

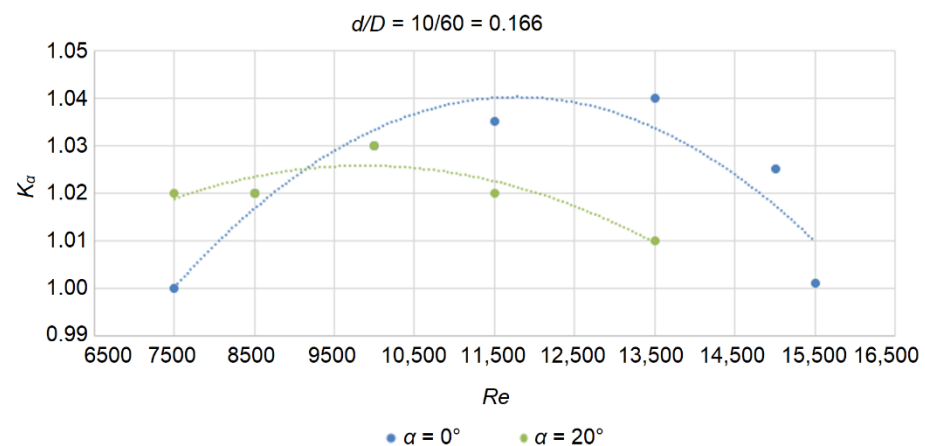


Figure 12. Dependence of the correction factors, K_{α} , on the criterion Re ($7000 < Re < 17,000$), with the ratio $d/D = 10/60 = 0.166$.

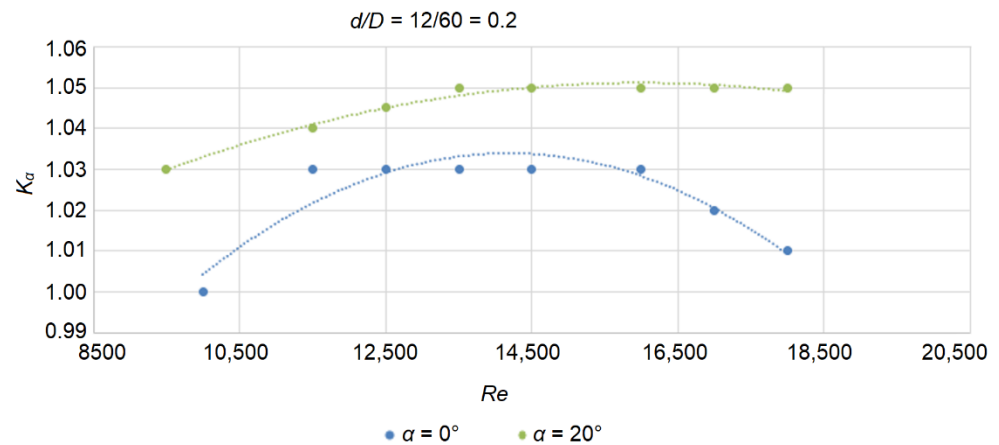


Figure 13. Dependence of the correction factors, K_{α} , on the criterion Re ($9000 < Re < 19,000$), with the ratio $d/D = 12/60 = 0.2$.

In the study of the dependence of the speed of movement of particles in the coil on the frequency of movement of the diaphragm of the pulsator, water was used as the washing liquid, and sand with an average particle size of $d_p = 2.58 \times 10^{-4}$ m was used as the dispersed particles. Data processing provided a graph of the dependence for the average velocity of particles in the coil on the frequency of movement of the diaphragm of the pulsator (Figure 14). It can be seen from the graph that, with an increase in frequency, to a certain value, the average speed of particles along the coil increases linearly, and with a further increase in frequency, the speed of the particles decreases. This is explained by the fact that, during the reverse stroke of the pulsator diaphragm, the granules move backward for a certain distance. Therefore, depending on the frequency of movement of the diaphragms of the pulsator, the washer can operate in two modes: either moving the granules or intensive mixing. The intensive mixing mode can be recommended for particles prone to sticking together.

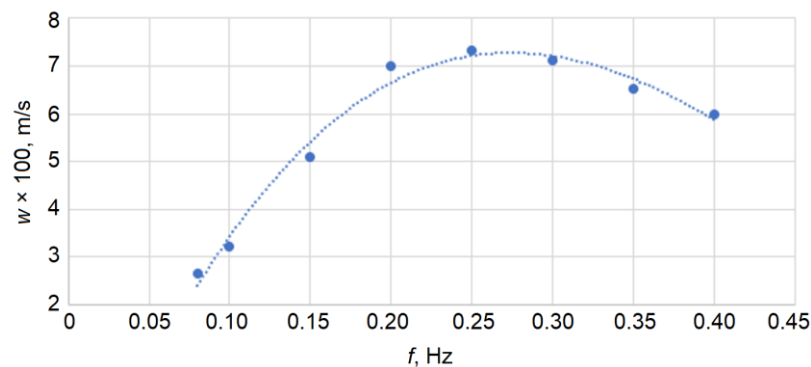


Figure 14. Dependence of the average speed of movement of the gel spheres in the washer coil on the frequency of movement of the diaphragm of the pulsator.

Based on the experimental data on condition monitoring, a graph of the dependence of the average speed of particle movement in the coil on the amplitude of diaphragm movement was also plotted (Figure 15). With an increase in the amplitude, the speed of particle movement increases linearly. However, at small amplitudes of movement of the diaphragms of the pulsator (in this case, 2.0 mm), a sharp decrease in the speed of the movement of particles and clogging of the coil by dispersed particles are observed. This is because low-intensity hydraulic impulses are damped by the liquid and air located in closed cavities. Therefore, the amplitude of movement of the diaphragm of the pulsator

must be greater than a certain minimum value, depending on the characteristics of the pulsator.

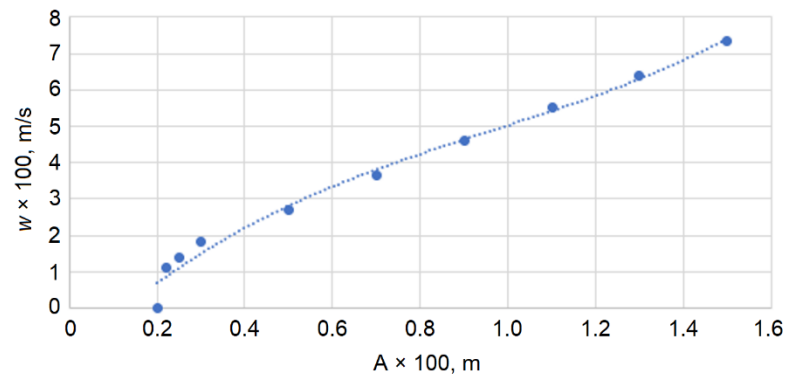


Figure 15. Dependence of the average speed of movement of the gel spheres in the washer coil on the amplitude of movement of the pulsator diaphragm.

Moreover, the dependence of the average speed of movement of particles in the coil on the average diameter of the coil was obtained (Figure 16). Since the change in speed is insignificant, the influence of the average diameter on the speed can be ignored in the calculations.

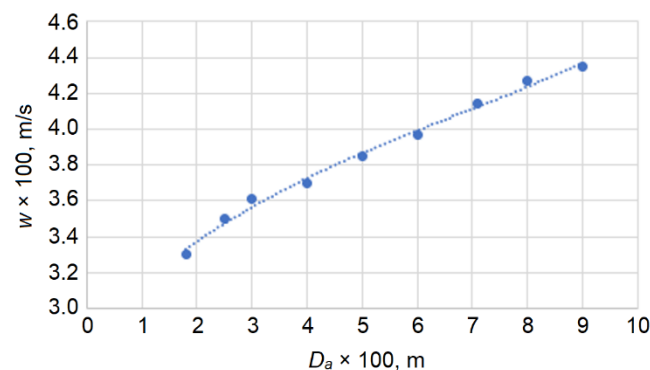


Figure 16. Dependence of the average speed of movement of the gel spheres in the washer coil on the average diameter of the coil.

When studying the dependence of the speed of movement of particles in the coil on the degree of filling of the coil with granules, it was found that the average speed of movement of particles depends on the degree of filling of the coil. If this degree is more than 0.4, the lower layers of particles lag the upper ones. Therefore, it is recommended to flush with a filling level of less than 0.4.

4. Discussion

The sol-gel method belongs to the condensation (“bottom-up”) approach to the production of powders and nanomaterials [30]. Comparison with other methods for materials production shows that the sol-gel method has the following advantages: a simplified synthesis flow scheme, reduced energy costs, and a high degree of products purity at all stages of synthesis with a minimum cost to achieve it, the possibility of purchasing a large specific surface, and as a result, improving the quality of the product, the product composition can be easily modified with dispersed additives and/or modifiers.

Obtaining a high surface area and stable surfaces is the essential advantage of the sol–gel method. The chemical and physical properties of the materials obtained by the sol–gel method are related to the experimental conditions applied [31].

Experimental batches of Al_2O_3 catalyst carrier gel spheres with a diameter of 1.0–3.0 mm were produced, and their strength and bulk density after drying and calcination were determined depending on the operating mode of the vibration granulator, namely, on the basket rotation frequency and oscillation frequency, and nitric acid concentration and powder–acid ratio ($\text{Al}(\text{OH})_3\text{:HNO}_3$). Studies of the physico-mechanical properties of Al_2O_3 granules showed that, with a decrease in the diameter of the dispersant holes from 1.4 to 1.2 mm and the vibration frequency of the vibrator from 100 to 40 Hz, the granulometric composition of the granules changes insignificantly. With a decrease in the oscillation frequency to 70–80 Hz, the limits of particle size distribution are 2.0 to 2.2 mm, and then, with a further decrease in the oscillation frequency to 40 Hz, the limits slightly increase and are 2.0 to 2.4 mm. It was found that, with a diameter of the disperser holes of 0.85 mm and an oscillation frequency of 100 Hz, the limits of the granulometric composition of the obtained granules are slightly changed to 1.2–2.0 mm, but most of the granules of Al_2O_3 are monodisperse aluminum with a diameter of 1.6 mm. Studies of the influence of the nitric acid concentration have shown that, with a powder–acid ratio of 1.05 to 2.0, the maximum value of the strength of the granule (1.8 kg/gran.) is achieved. It was also determined that the optimal mode for forming monodisperse granules with the highest bulk density is the mode of operation of the dispersant at an oscillation frequency of 68 Hz and a hole diameter of 1.2 mm.

Recommendations for determining the flow coefficient, μ , give a discrepancy with the results of the experiments on condition monitoring, especially at low Reynolds numbers ($\text{Re} < 10^5$). For a more accurate determination of the coefficient μ , it is advisable to use the correction factors, K_μ . Physical experiments determined the values of these coefficients for different values of the ratio of d/D .

Physical simulations of processes occurring in coil pulsation washers showed that, at a frequency of 0.2 to 0.3 Hz, the highest speed of movement of the granules is observed, approximately 0.07 m/s. In this case, the speed of movement of the spheres increases linearly with an increase in the amplitude of the movement of the pulsator. It should be noted that this study did not determine the efficiency of cleaning gel spheres, so in the future, we plan to determine the dependence of the cleaning efficiency on the speed of movement of the granules in the coil.

The obtained results are consistent with the data [32–34] regarding the obtained microspheres Al_2O_3 , e.g., granule size, powder/acid ratio ($\text{Al}(\text{OH})_3\text{:HNO}_3$), and strength of granules. Moreover, these results are consistent with the data of the References [35,36], where the dataset regarding the pore sizes and the specific surface area of the granules is given.

Further studies will be aimed at conducting a morphological analysis by using scanning electron microscopy (SEM) and obtaining an element composition of the granules under different hydrodynamic conditions, with various initial compositions, using energy dispersive X-ray analysis (EDX).

5. Conclusions

A technique for conducting physical experiments on the process of dispersing a liquid (sol) was presented that allows for the evaluation of the effect of hydrodynamic parameters and design parameters of equipment on the physical and mechanical properties of the resulting Al_2O_3 catalyst granules. For experimental studies, setups for producing an Al_2O_3 catalyst and for studying the process of liquid leakage from the openings of a dispersing device (priller) were developed, and a pulsating-washer design was proposed.

For carrying out condition monitoring, experimental batches of Al_2O_3 catalyst carrier gel spheres with a diameter of 1.0 to 3.0 mm were produced, and their strength and bulk density after drying and calcination were determined depending on the operating mode of the priller, namely on the basket rotation frequency and oscillation frequency; the nitric acid concentration; and the powder–acid ratio ($\text{Al}(\text{OH})_3:\text{HNO}_3$). It was found that, with disperser holes of 0.85 mm in diameter and an oscillation frequency of 100 Hz, the limits of the granulometric composition of the obtained granules are slightly increased from 1.2 to 2.0 mm, but most of the granules of Al_2O_3 are monodisperse aluminum with a diameter of 1.6 mm. Studies of the influence of the concentration of nitric acid have shown that when the powder–acid ratio is 1.05 to 2.0, the maximum value of the strength of the granule (1.8 kg/gran.) is achieved.

Studies of the process of fluid leakage from the hole established that the circulation in the reservoir significantly affects the volumetric flow rate of the liquid through the hole. For example, an increase in the circumferential velocity of the vortex during circulation reduces the flow rate of the liquid through the hole. So, at an overpressure above the hole equal to 1.15 MPa and circulation of $0.77 \text{ m}^2/\text{s}$, the volumetric flow rate of the sol through the hole is 0.037 L/s, and in the absence of circulation in the glass, the flow rate is 0.106 L/s, which is also confirmed by other experiments.

The dependence of the speed of movement of the gel spheres on the frequency of movement of the diaphragm of the pulsator, on the amplitude of movement of the diaphragm of the pulsator, on the average diameter of the coil, and on the degree of filling of the coil with granules was determined from the results of the physical experiments.

Author Contributions: Conceptualization, V.S. and O.L.; funding acquisition, J.P.; methodology, K.S., I.P., M.S. and R.O.; investigation, K.S., M.S. and M.V.; writing—original draft preparation, O.S., M.D. and O.M.; software, O.L., M.D. and O.Y.; supervision and formal analysis, I.P. and J.P.; project administration, V.S.; writing—review and editing, M.Y., O.S. and O.M.; data curation, R.O. and O.Y.; resources, M.Y. and M.V. All authors have read and agreed to the published version of the manuscript.

Funding: This work was supported by the Slovak Research and Development Agency, under the contract No. APVV-19-0590; and by the projects VEGA 1/0704/22 and KEGA 055TUKE-4/2020, granted by the Ministry of Education, Science, Research and Sport of the Slovak Republic.

Institutional Review Board Statement: Not applicable.

Informed Consent Statement: Not applicable.

Data Availability Statement: Not applicable.

Acknowledgments: The scientific results were achieved within the project “Creation of new granular materials for nuclear fuel and catalysts in the active hydrodynamic environment” (State reg. No. 0120U102036), ordered by the Ministry of Education and Science of Ukraine.

Conflicts of Interest: The authors declare no conflict of interest.

Appendix A

Results of experiments

| Ratio of d/D | Height of the Liquid Column above the Hole, h (m) | Circulation in a Glass, G (m ² /s) | the Flow Rate through the Hole, Q (L/s) |
|----------------|---|---|---|
| 0.0635 | 26 | 0 | 0.0090 |
| | | 0.250 | 0.0040 |
| | 58 | 0 | 0.0130 |
| | | 0.135 | 0.0053 |
| | 90 | 0 | 0.0162 |
| | | 0.107 | 0.0058 |
| 120 | 0 | 0.0187 | |
| | 0.165 | 0.0120 | |
| 0.1330 | 28 | 0 | 0.2300 |
| | | 0.379 | 0.0080 |
| | 55 | 0 | 0.0320 |
| | | 0.313 | 0.0098 |
| | 66 | 0 | 0.0350 |
| | | 0.300 | 0.0120 |
| 96 | 0 | 0.0425 | |
| | 0.500 | 0.0197 | |
| 120 | 0 | 0.0475 | |
| | 0.536 | 0.0263 | |
| 0.1670 | 40 | 0 | 0.0428 |
| | | 0.244 | 0.0067 |
| | 53 | 0 | 0.0495 |
| | | 0.348 | 0.0109 |
| | 75 | 0 | 0.0590 |
| | | 0.272 | 0.0161 |
| 94 | 0 | 0.0655 | |
| | 0.605 | 0.0232 | |
| 112 | 0 | 0.0720 | |
| | 0.605 | 0.0278 | |
| 0.2000 | 43 | 0 | 0.0640 |
| | | 0.755 | 0.0133 |
| | 54 | 0 | 0.0730 |
| | | 0.780 | 0.0173 |
| | 62 | 0 | 0.0740 |
| | | 0.860 | 0.0218 |
| 85 | 0 | 0.0900 | |
| | 0.775 | 0.0270 | |
| 117 | 0 | 0.1060 | |
| | 0.770 | 0.0370 | |

References

1. Sood, D.D. The role sol-gel process for nuclear fuels-an overview. *J. Sol-Gel Sci. Technol.* **2010**, *59*, 404–416. [[CrossRef](#)]
2. Dimitriev, Y.; Ivanova, Y.; Iordanova, R. History of sol-gel science and technology. *J. Univ. Chem. Technol. Metall.* **2008**, *43*, 181–192.
3. Mao, N.; Du, M. Sol-gel-based treatments of textiles for water repellence. *Waterproof Water Repel. Text. Cloth.* **2018**, 233–265. [[CrossRef](#)]
4. Chatzistavrou, X.; Kontonasaki, E.; Paraskevopoulos, K.M.; Koidis, P.; Boccaccini, A.R. Sol-gel derived bioactive glass ceramics for dental applications. *Non-Met. Biomater. Tooth Repair Replace.* **2013**, 194–231. [[CrossRef](#)]
5. Lackey, W.J.; Blanco, R.E.; Lotts, A.L. Application of Sol-Gel Technology to Fixation of Nuclear Reactor Waste. *Nucl. Technol.* **1980**, *49*, 321–324. [[CrossRef](#)]
6. Vaidya, V.N. Status of sol-gel process for nuclear fuels. *J. Sol-Gel Sci. Technol.* **2008**, *46*, 369–381. [[CrossRef](#)]
7. Demianenko, M.; Volf, M.; Skydanenko, M.; Yakovchuk, V.; Pavlenko, I.; Liaposhchenko, O. Numerical Simulation of the Perforated Shell's Oscillations in a Vibrational Priller. *J. Eng. Sci.* **2020**, *7*, F30–F36. [[CrossRef](#)]
8. Durães, L.; Benedini, L.; Costa, B.F.O.; Portugal, A. Sol-gel synthesis and washing of amorphous g-FeO(OH) xerogels. *Mater. Werkst.* **2012**, *43*, 427–434. [[CrossRef](#)]
9. Yamagishi, S.; Takahashi, Y. Behavior and Removal of Impurity Sulphate in Sol-Gel Process for ThO₂ and (Th, U)O₂ Microsphere Fabrication. *J. Nucl. Sci. Technol.* **1989**, *26*, 939–947. [[CrossRef](#)]
10. Ganguly, C. Sol-gel microsphere pelletization: A powder-free advanced process for fabrication of ceramic nuclear fuel pellets. *Bull. Mater. Sci.* **1993**, *16*, 509–522. [[CrossRef](#)]
11. Brykala, M.; Rogowski, M.; Wawszczak, D.; Olczak, T.; Smolinski, T. Microspheres and Pellets of UO₂ Prepared Via ADU by Complex Sol-Gel Process and ICHTJ Process. *Arch. Metall. Mater.* **2020**, *65*, 1397–1404.
12. Brykala, M.; Walczak, R.; Wawszczak, D.; Kilim, S.; Rogowski, M.; Strugalska-Gola, E.; Szuta, M. Preparation by the double extraction process with preliminary neutron irradiation of yttria or calcia stabilised cubic zirconium dioxide microspheres. *Nucl. Eng. Technol.* **2021**, *53*, 188–198. [[CrossRef](#)]
13. Katalenich, J.A. Production of Monodisperse, Crack-Free Cerium Oxide Microspheres by Internal Gelation Sol-Gel Methods. Ph.D. Thesis, University of Michigan, Ann Arbor, MI, USA, 2014; 277p.
14. Song, T.; Guo, L.; Chen, M.; Chang, Z.Q. Influences of heating processes on properties and microstructure of porous CeO₂ beads as a surrogate for nuclear fuels fabricated by a microfluidic sol-gel process. *Nucl. Eng. Technol.* **2019**, *51*, 257–262. [[CrossRef](#)]
15. Yadav, S.; Gaikwad, G.; Chaturvedi, A.; Ananthasivan, K.; Pandit, A.; Jain, R. Fabrication of CeO₂ microspheres by internal gelation process using T junction droplet generator. *Braz. J. Chem. Eng.* **2022**, *39*, 671–689. [[CrossRef](#)]
16. Pan, Y. The influence of ag and cu on the electronic and optical properties of ZrO from first-principles calculations. *Mater. Sci. Semicond. Process.* **2021**, *135*, 106084. [[CrossRef](#)]
17. Smyrnioti, M.; Ioannides, T. Dimethyl ether oxidation over copper ferrite catalysts. *Catalysts* **2022**, *12*, 604. [[CrossRef](#)]
18. Pan, Y.; Yu, E. New insight into the structural and physical properties of AlH₃. *Int. J. Energy Res.* **2022**. [[CrossRef](#)]
19. Pu, D.; Pan, Y. First-principles investigation of oxidation mechanism of Al-doped Mo₅Si₃ silicide. *Ceram. Int.* **2022**, *48*, 11518–11526. [[CrossRef](#)]
20. Hu, B.; Jia, E.; Du, B.; Yin, Y. A new sol-gel route to prepare dense Al₂O₃ thin films. *Ceram. Int.* **2016**, *42*, 16867–16871. [[CrossRef](#)]
21. Su, Z.; Yao, M.; Li, M.; Gao, W.; Li, Q.; Feng, Q.; Yao, X. A novel and simple aluminium/sol-gel-derived amorphous aluminium oxide multilayer film with high energy density. *J. Mater. Chem. C* **2018**, *6*, 5616–5623. [[CrossRef](#)]
22. Chokkalingam, V.; Seemann, R.; Weidenhof, B.; Maier, W.F. Droplet-based microfluidic scheme for complex chemical reactions. In *Advances in Microfluidics*; Kelly, R., Ed.; IntechOpen: London, UK, 2012; pp. 77–96. [[CrossRef](#)]
23. Ganguli, C.; Langen, H.; Zimmer, E.; Mertz, E.R. Sol-Gel microsphere pelletization process for fabrication of high-density ThO₂–2% UO₂ fuel for advanced pressurized heavy water reactors. *Nucl. Technol.* **2017**, *73*, 84–95. [[CrossRef](#)]
24. Kumar, N.; Sharma, R.K.; Ganatra, V.R.; Mukerjee, S.K.; Vaidya, V.N.; Sood, D.D. Studies of the Preparation of Thoria and Thoria-Urania Microspheres Using an Internal Gelation Process. *Nucl. Technol.* **2017**, *96*, 169–177. [[CrossRef](#)]
25. Ben-Arfa, B.A.E.; Salvado, I.M.M.; Ferreira, J.M.F.; Pullar, R.C. Novel route for rapid sol-gel synthesis of hydroxyapatite, avoiding ageing and using fast drying with a 50-fold to 200-fold reduction in process time. *Mater. Sci. Eng. C* **2017**, *70*, 796–804. [[CrossRef](#)] [[PubMed](#)]
26. Skydanenko, M. Analyzing hydrodynamics in hollow perforated shell of centrifugal oscillating granulator. *East.-Eur. J. Enterp. Technol.* **2014**, *3*, 30–35. [[CrossRef](#)]
27. Pavlenko, I.; Sklabinskyi, V.; Doligalski, M.; Ochowiak, M.; Mrugalski, M.; Liaposhchenko, O.; Skydanenko, M.; Ivanov, V.; Włodarczak, S.; Woziwodzki, S.; et al. The mathematical model for the secondary breakup of dropping liquid. *Energies* **2020**, *13*, 6078. [[CrossRef](#)]
28. Yurchenko, O.; Sklabinskyi, V.; Ochowiak, M.; Ostroha, R.; Gusak, O. Rational choice of a basket for the rotational vibropriller. *J. Eng. Sci.* **2022**, *9*, F16–F20. [[CrossRef](#)]
29. Pavlenko, I.; Sklabinskyi, V.; Pitel', J.; Židek, K.; Kuric, I.; Ivanov, V.; Skydanenko, M.; Liaposhchenko, O. Effect of superimposed vibrations on droplet oscillation modes in prilling process. *Processes* **2020**, *8*, 566. [[CrossRef](#)]
30. Nikolayev, V.A. Sol-Gel Synthesis of Various Types of Nanomaterials Based on Titanium Dioxide and Carbide. Ph.D. Thesis, Institute of General and Inorganic Chemistry, Moscow, Russia, 2018.

31. Yilmaz, E.; Soylak, M. Functionalized nanomaterials for sample preparation methods. In *Handbook of Nanomaterials in Analytical Chemistry*; Hussain, C.M., Ed.; Elsevier: Amsterdam, The Netherlands, 2020; pp. 375–413.
32. Buelna, G.; Lin, Y.S. Sol–gel-derived mesoporous γ -alumina granules. *Microporous Mesoporous Mater.* **1999**, *30*, 359–369. [[CrossRef](#)]
33. Deng, S.G.; Lin, Y.S. Granulation of sol–gel-derived nanostructured alumina. *AIChE J.* **1997**, *43*, 505–514. [[CrossRef](#)]
34. Kureti, S.; Weisweiler, W. A novel sol–gel method for the synthesis of γ -aluminium oxide: Development of the sol–gel transformation and characterization of the xerogel. *J. Non-Cryst. Solids* **2002**, *303*, 253–261. [[CrossRef](#)]
35. Choi, J.; Kim, B.; Kim, J. Structural evolution of sol–gel derived nanostructured alumina granules with calcination temperature. *J. Chem. Eng. Jpn.* **2006**, *39*, 1000–1003. [[CrossRef](#)]
36. Yadav, A.K.; Bhattacharyya, S. A new approach for the fabrication of porous alumina beads using acid leachate of kaolin. *Microporous Mesoporous Mater.* **2020**, *293*, 109795. [[CrossRef](#)]